Figure S1. Meta-analysis. (A) Article selection process. Search terms were used to identify studies including patients undergoing curative surgery for stage I-III CRC, with metastasis-free survival assessed based on the KRAS mutation status. (B) Funnel plots showing publication bias. CRC, colorectal cancer; MFS, metastasis-free survival.

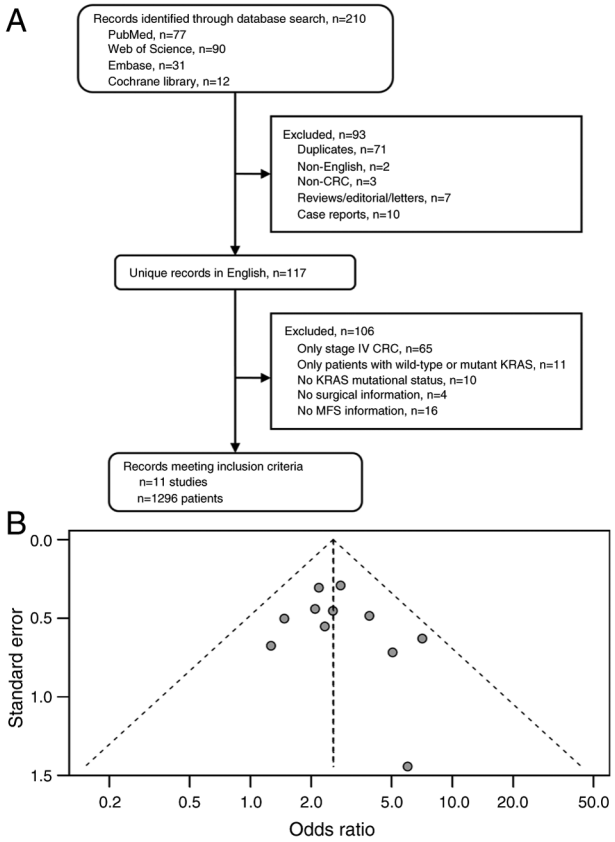

Figure S2. Inclusion and exclusion of databases in the metastasis-free survival analysis. (A) ICGC-ARGO, (B) MSKCC and (C) Sidra-LUMC AC-ICAM flowchart. ICGC-ARGO, International Cancer Genome Consortium Accelerating Research in Genomic Oncology; MSKCC, Memorial Sloan-Kettering Cancer Center; LUMC AC-ICAM, Leiden University Medical Center Atlas and Compass of Immune-Cancer-Microbiome interactions; CRC, colorectal cancer.

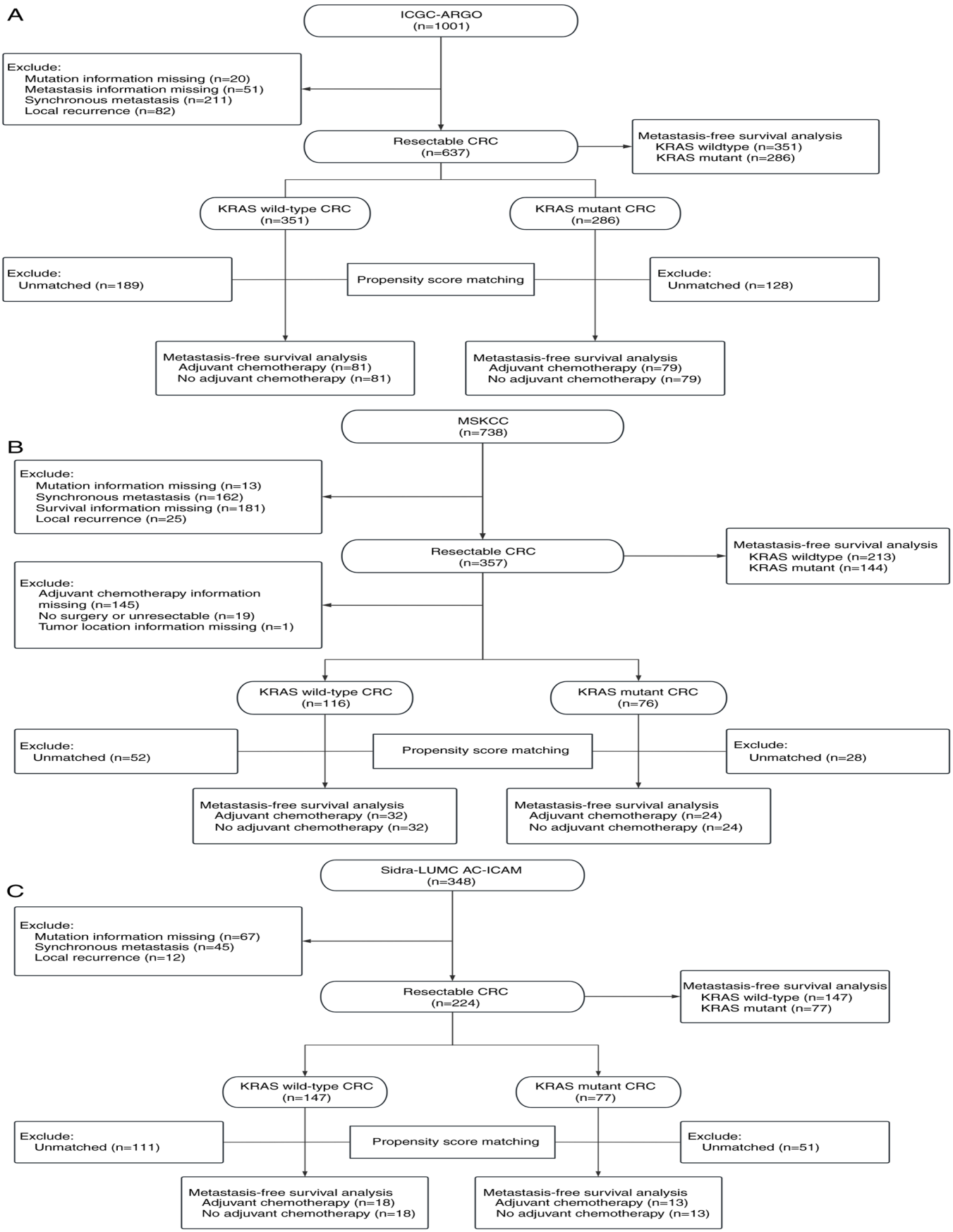

Figure S3. KRAS metachronous metastasis risk prediction model. (A) Optimization of λ) for the Lasso-COX model. (B) Gene feature coefficients of the metastasis risk prediction model. The cutoff values for determining high-risk and low-risk groups based on the Youden index were determined for each cohort (ARGO, -0.2184; Sidra-LUMC AC-ICAM, -0.0362; MSKCC, -31.1379). (C) Coefficient trace plot of the variable selection process of the Lasso-COX model. (D) Differentially expressed genes of epithelial-mesenchymal transition and TGF-β pathways between patients with high and low risk MSKCC and AC-ICAM KRAS-MUT CRC. ARGO, Accelerating Research in Genomic Oncology; LUMC AC-ICAM, Leiden University Medical Center Atlas and Compass of Immune-Cancer-Microbiome interactions; MSKCC, Memorial Sloan-Kettering Cancer Center.

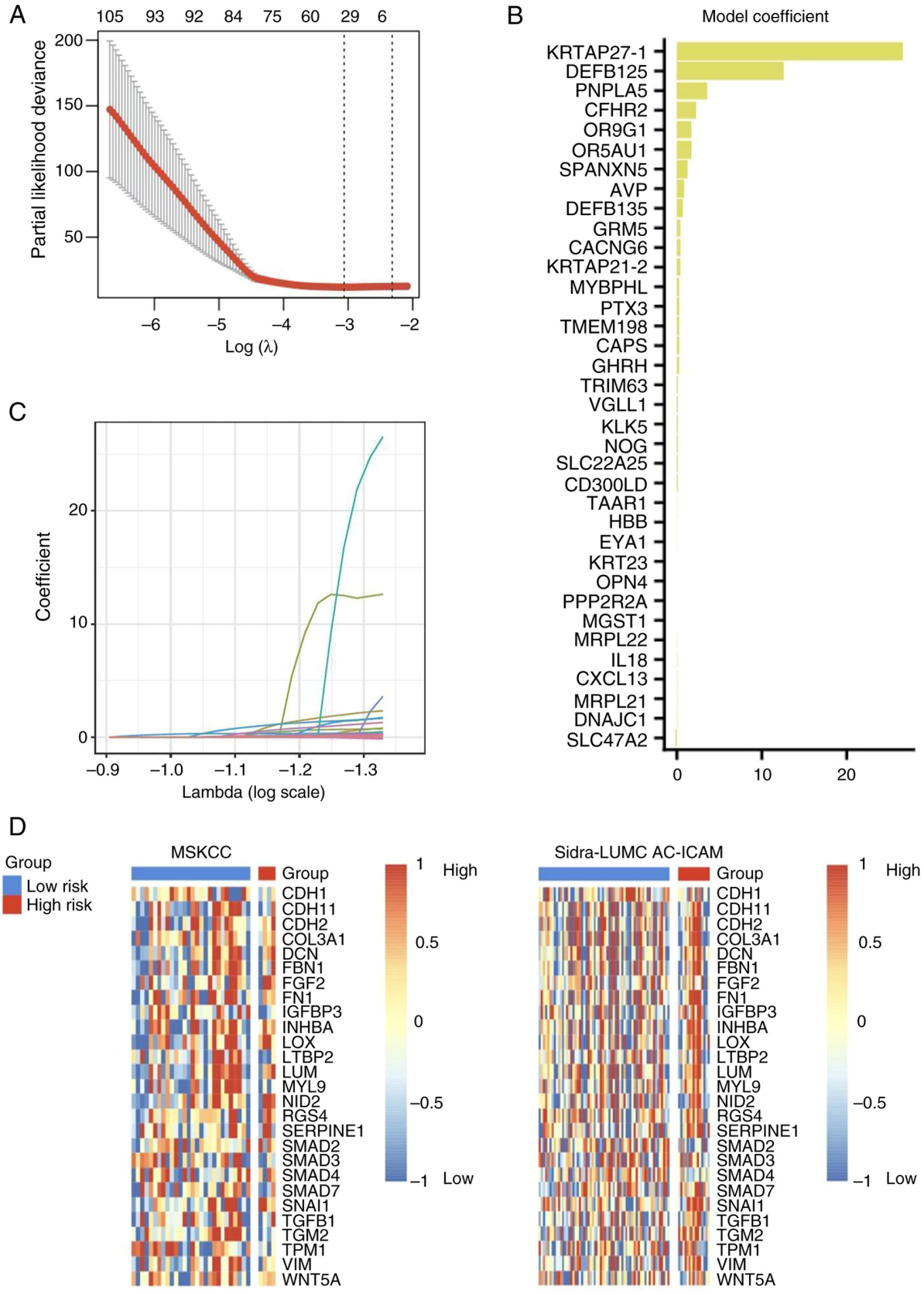

Figure S4. IC50 of chemotherapy for CRC cell lines. The CRC cell lines were treated with (A) 5-fluorouracil and (B) oxaliplatin. CRC, colorectal cancer; IC50, half-maximal inhibitory concentration.

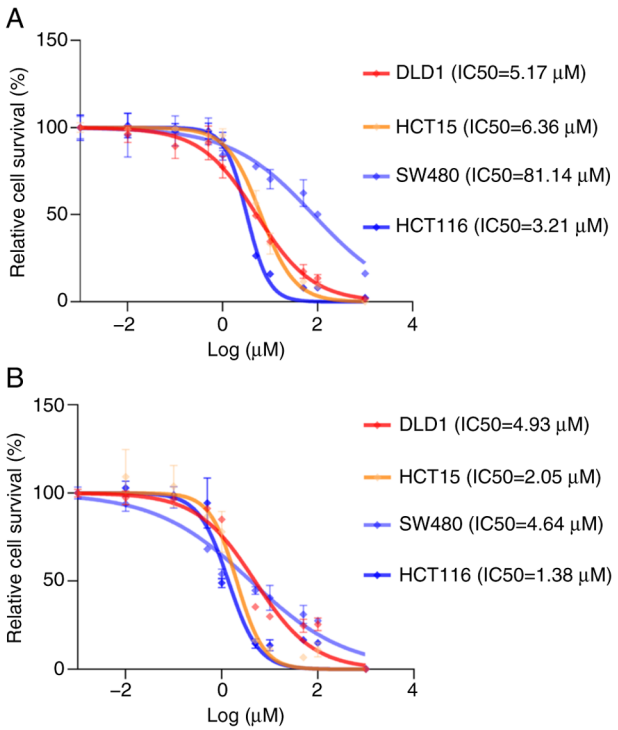

Figure S5. Inhibitory effect of chemo on colorectal cell lines. The effect of chemo on migration and invasion of DLD1 was examined using (A) wound healing assay (A) and Transwell assay (B). The effect of chemo on migration and invasion of HCT15 was assessed using wound healing assay (C) and Transwell assay (D). The effect of chemo on migration and invasion of SW480 was assessed using wound healing assay (E) and Transwell assay (F). The effect of chemo on migration and invasion of HCT116 was assessed using wound healing assay (G) and Transwell assay (H). Scale bar, 200 μm. ***P<0.001. ns, not significant; chemo, chemotherapy.

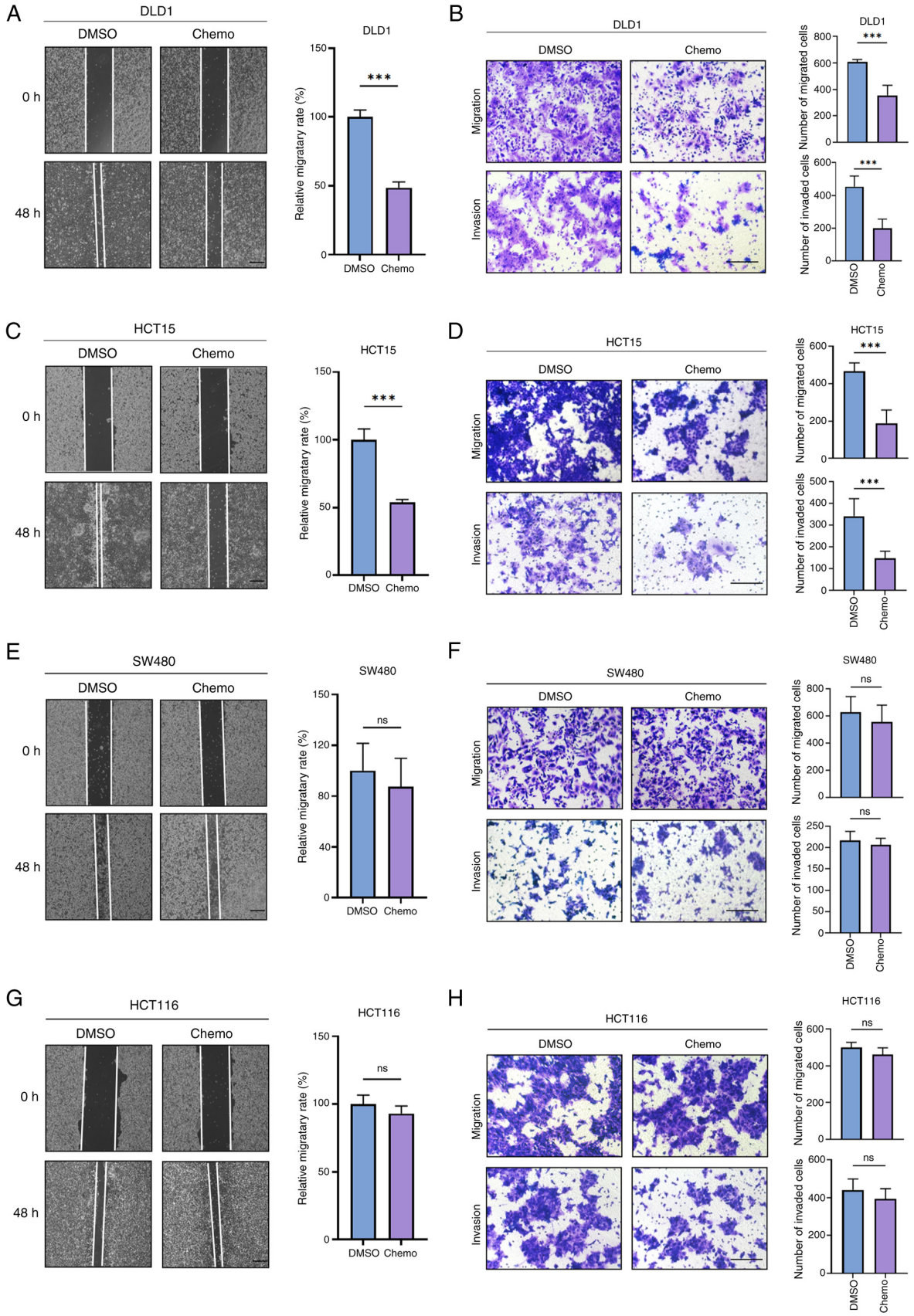

Figure S6. CRC cell lines morphology. (A) Morphology of SW620 and SW480. Magnification, 100x. (B) GSEA of Hallmark in GSE228010 showing enrichment of the EMT pathway. (C) Effect of KRASi on the morphology of colorectal cancer cell lines. Magnification, 100x. KRASi, KRAS inhibitor.

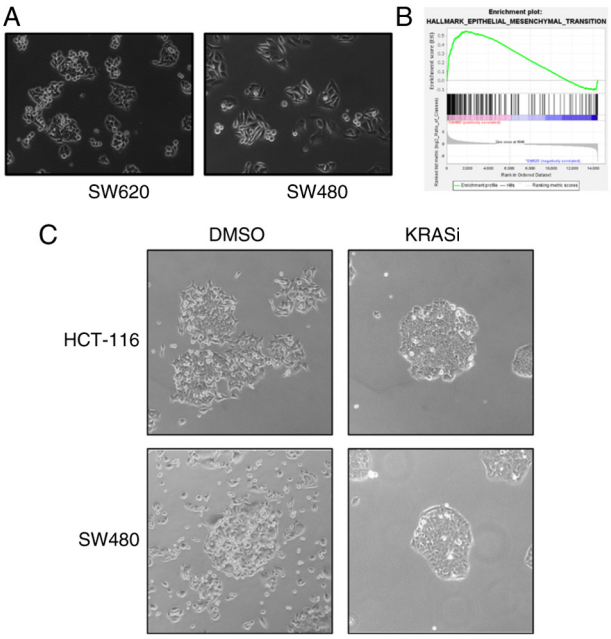

Figure S7. Induction and validation of adagrasib acquired resistance in SW837 cells. (A) Long-term treatment effect of adagrasib modeling in KRAS-G12C mutant CRC cell line SW837. (B) Colony formation assay of SW837-P and SW837-R cells. (C) Growth curve of SW837-P and SW837-R cells treated with adagrasib (500 nM). (D) Viability of SW837-P and SW837-R cell lines treated with the indicated concentrations of adagrasib. (E) Immunoblot analysis of ERK proteins in SW837-P/R cells treated with adagrasib for 1 h. ***P<0.001. P, parental; R, resistant; IC50, half-maximal inhibitory concentration; p-, phospho-.

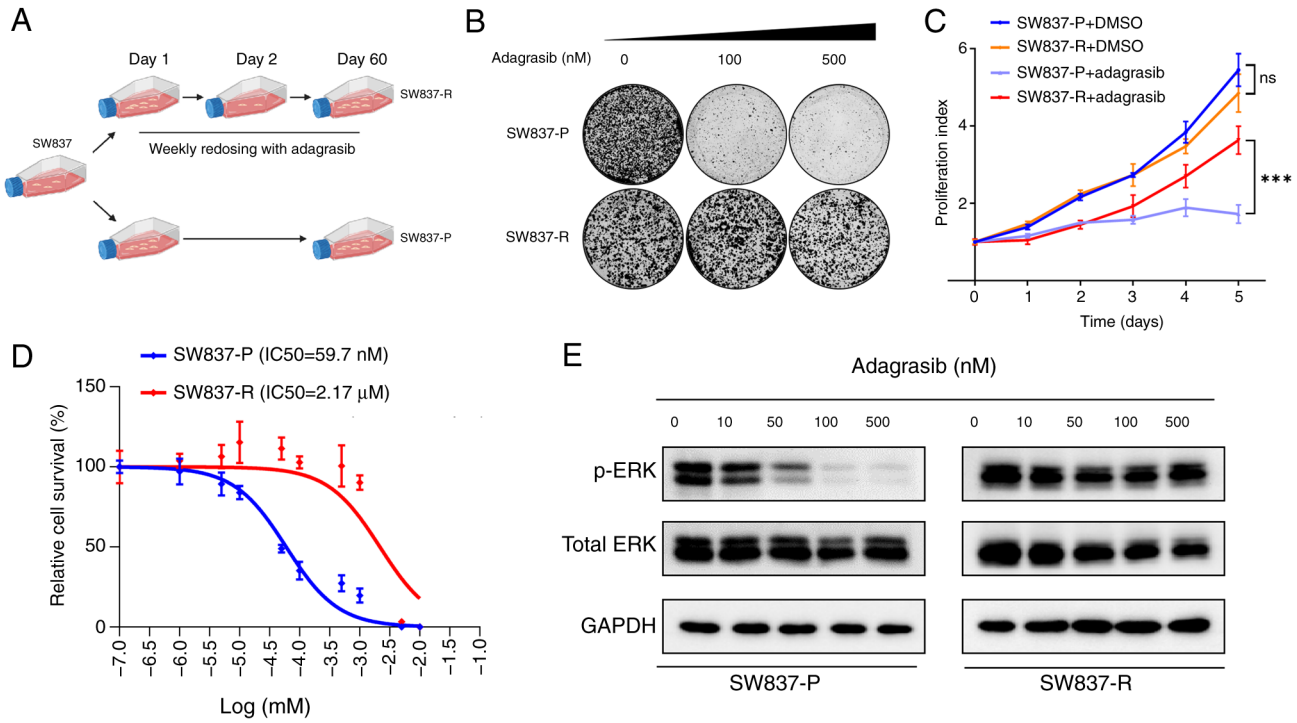

Figure S8. Mouse body weight. Ctrl, control; KRASi, KRAS inhibitor.

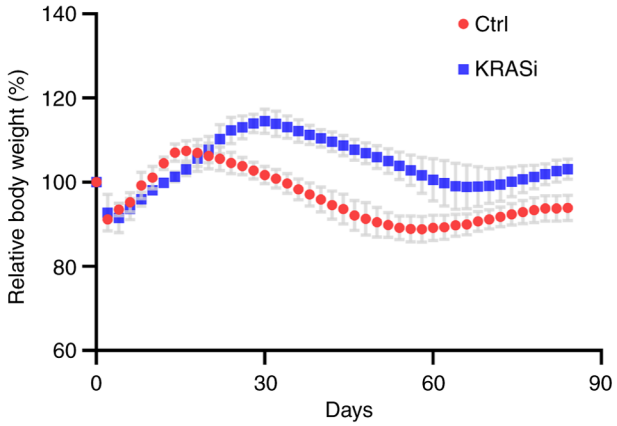

Relative body weight loss, %	Ctrl	KRASi
Maximum	14.96	11.71
Mean	12.08	10.12

Figure S9. Gene set enrichment analysis of the GSE116823 dataset. Hallmark pathway analysis for downregulated genes in HCT116 following KRAS knockdown. (A) Epithelial-mesenchymal transition and (B) TGF-β pathway enrichment plot. NES, normalized enrichment score.

A

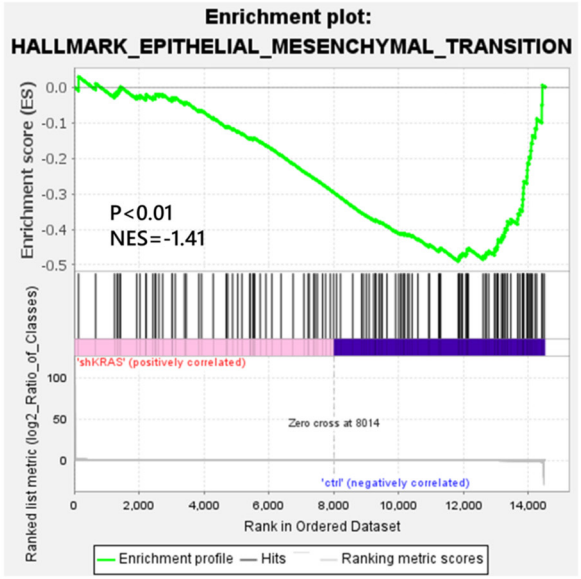

B